Analytical model of the nonlinear dynamics of cantilever tip-sample surface interactions for various acoustic atomic force microscopies

John H. Cantrell*
NASA Langley Research Center, Mail Stop 231, Hampton, Virginia 23681, USA

Sean A. Cantrell†
Department of Physics, University of Virginia, Charlottesville, Virginia 22904, USA

(Received 26 October 2007; revised manuscript received 3 March 2008; published 8 April 2008)

An analytical model is developed of the interaction of the cantilever tip of an atomic force microscope with the sample surface that treats the cantilever and sample as independent systems coupled by a nonlinear force acting between the cantilever tip and a volume element of the sample surface. To maintain equilibrium, the volume element is subjected to a restoring force from the remainder of the sample. The model accounts for the positions on the cantilever of the cantilever tip, laser probe, and excitation force (if any). The model leads to a pair of coupled nonlinear differential equations that are solved analytically using a matrix iteration procedure. Solutions are obtained for the phase and amplitude signals generated by various acoustic atomic force microscope (A-AFM) techniques including force modulation microscopy, atomic force acoustic microscopy, ultrasonic force microscopy, heterodyne force microscopy, resonant difference-frequency atomic force ultrasonic microscopy (RDF-AFUM), and amplitude modulation–atomic force microscopy (AM-AFM) (intermittent contact mode). The solutions are used to obtain a quantitative measure of A-AFM image contrast resulting from variations in the Young modulus of the sample. Applications of the model to measurements of LaRC™-CP2 polyimide film using RDF-AFUM and AM-AFM images predict maximum variations in the Young modulus of 24% and 18%, respectively, over a common scan area. Both predictions are in good agreement with the value of 21% obtained from independent mechanical stretching measurements of the polyimide sheet material.

DOI: 10.1103/PhysRevB.77.165409 PACS number(s): 68.37.Ps, 68.37.Tj, 81.40.Jj, 62.30.+d

I. INTRODUCTION

The atomic force microscope[1] (AFM) has become an important nanoscale characterization tool for the development of materials and devices. Dynamic implementations of the AFM (we shall call acoustic atomic force microscopies or A-AFM) such as amplitude modulation–atomic force microscopy (AM-AFM) (also called intermittent contact mode or tapping mode), force modulation microscopy (FMM),[2] atomic force acoustic microscopy (AFAM),[3,4] ultrasonic force microscopy,[5,6] heterodyne force microscopy (HFM),[7,8] resonant difference-frequency atomic force ultrasonic microscopy (RDF-AFUM)[9] and variations of these techniques[10–16] utilize the interaction force between the cantilever tip and the sample surface to extract information about sample material properties. Such properties include sample elastic moduli, adhesion, surface viscoelasticity, embedded particle distributions, and topography. The cantilever tip-sample surface interaction force is generally nonlinear, although in some operational modes the interaction force can be taken to a good approximation to be linear.

Various approaches to assessing the nonlinear behavior of the cantilever probe dynamics have been published.[5,6,17–26] We consider here a general, yet detailed, analytical treatment of the cantilever and the sample as independent systems in which the interaction force provides a coupling between the cantilever tip and the small volume element of sample surface involved in the coupling. The sample volume element is itself subject to a restoring force from the remainder of the sample. The coupling includes the lowest-order terms in the nonlinearity. Such terms are sufficient to account for the most important operational characteristics and material properties obtained from each of the various acoustic atomic force microscopies cited above. A particular advantage of the coupled independent system model is that the equations are valid for all regions of the force-separation curve and emphasize the local curvature properties (functional form) of the curve. Another advantage is that the dynamics of the sample, hence energy transfer characteristics, can be extracted straightforwardly from the solution set using the same mathematical procedure as that for the cantilever.

We begin in Sec. II by developing a mathematical model of the interaction between the cantilever tip and the sample surface that involves a coupling via the nonlinear interaction force of separate dynamical equations for the cantilever and the sample surface. A general solution that accounts for the positions of the excitation force (e.g., a piezotransducer) and the cantilever tip along the length of the cantilever as well as for the position of the laser probe on the cantilever surface is found. The solution contains static terms (including static terms generated by the nonlinearity), linear oscillatory terms, and nonlinear oscillatory terms. Individual or various combinations of these terms are shown in Sec. III to apply as appropriate to a description of a given A-AFM modality cited above. Section IV provides a quantitative analysis of image contrast for each of the A-AFM techniques. In order to test the validity of the present model, comparative measurements of the maximum fractional variation of the Young modulus in a film of LaRC™-CP2 polyimide polymer are presented in Sec. V using the RDF-AFUM and AM-AFM modalities. The two modalities represent opposite extremes in measurement complexity, both in instrumentation and in

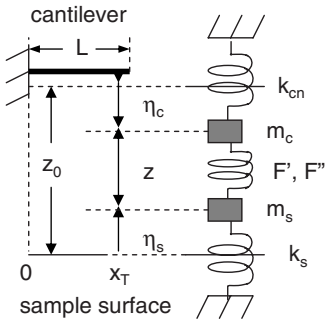

FIG. 1. Schematic of cantilever tip-sample surface interaction: z_0 is the quiescent tip-surface separation distance, z the oscillating tip-surface separation distance, η_c the displacement (positive down) of the cantilever tip, η_s the displacement of the sample surface (positive up), k_{cn} is the nth mode cantilever stiffness constant (represented as an nth mode spring), m_c the cantilever mass, k_s the sample stiffness constant (represented as a single spring), m_s the active sample mass, and $F'(z_0)$ and $F''(z_0)$ are the linear and first-order nonlinear interaction force stiffness constants, respectively.

the analytical expressions used to calculate the variation in the Young modulus.

II. ANALYTICAL MODEL OF NONLINEAR CANTILEVER DYNAMICS

A. General dynamical equations

The cantilever of the AFM is able to vibrate in a number of different modes in free space corresponding to various displacement types (flexural, longitudinal, shear, etc.), resonant frequencies, and effective stiffness constants. Although any shape or oscillation mode of the cantilever can in principle be used in the analysis to follow, for definiteness and expediency we consider only the flexural modes of a cantilever modeled as a rectangular, elastic beam of length L, width a, and height b. We assume the beam to be clamped at the position $x=0$ and unclamped at the position $x=L$, as indicated in Fig. 1. We consider the flexural displacement $y(x,t)$ of the beam to be subjected to some general force per unit length $H(x,t)$, where x is the position along the beam and t is time. The dynamical equation for such a beam is[27]

$$E_B I \frac{\partial^4 y(x,t)}{\partial x^4} + \rho_B A_B \frac{\partial^2 y(x,t)}{\partial t^2} = H(x,t), \tag{1}$$

where E_B is the elastic modulus of the beam, $I=ab^3/12$ is the bending moment of inertia, ρ_B is the beam mass density, and $A_B=ab$ is the cross-sectional area of the beam.

The solution to Eq. (1) may be obtained as a superposition of the natural vibrational modes of the unforced [i.e., $H(x,t)=0$] cantilever as

$$y(x,t) = \sum_{n=1}^{\infty} Y_n(x)\,\eta_{cn}(t), \tag{2}$$

where the spatial eigenfunctions $Y_n(x)$ form an orthogonal basis set given by[27]

$$Y_n(x) = \left(\frac{\sin q_n x - \sinh q_n x}{\cos q_n x + \cosh q_n x}\right)(\sin q_n x - \sinh q_n x) + (\cos q_n x - \cosh q_n x). \tag{3}$$

The flexural wave numbers q_n in Eq. (3) are determined from the boundary conditions as $\cos(q_n L)\cosh(q_n L)=-1$ and are related to the corresponding modal angular frequencies ω_n via the dispersion relation $q_n^4=\omega_n^2\rho_B A_B/E_B I$. The general force per unit length $H(x,t)$ can also be expanded in terms of the spatial eigenfunctions as[28]

$$H(x,t) = \sum_{n=1}^{\infty} B_n(t) Y_n(x). \tag{4}$$

Applying the orthogonality condition

$$\int_0^L Y_m(x) Y_n dx = L\delta_{mn} \tag{5}$$

(δ_{mn} are the Kronecker deltas) to Eq. (4), we obtain

$$B_n(t) = \int_0^L H(\xi,t) Y_n(\xi) d\xi. \tag{6}$$

We now assume that the general force per unit length acting on the cantilever is composed of (1) a cantilever driving force per unit length $H_c(x,t)$, (2) an interaction force per unit length $H_T(x,t)$ between the cantilever tip and the sample surface, and (3) a dissipative force per unit length $H_d(x,t)$. Thus, the general force per unit length $H(x,t)=H_c(x,t)+H_T(x,t)+H_d(x,t)$. We now assume that the driving force per unit length is a purely sinusoidal oscillation of angular frequency ω_c and magnitude P_c. We also assume the driving force to result from a drive element (e.g., a piezotransducer) applied at the point x_c along the cantilever length. We thus write $H_c(x,t)=P_c e^{i\omega_c t}\delta(x-x_c)$, where $\delta(x-x_c)$ is the Dirac delta function. The interaction force per unit length $H_T(x,t)$ of magnitude P_T is applied at the cantilever tip at $x=x_T$ and is not a direct function of time, since it serves as a passive coupling between the independent cantilever and sample systems. We thus write the interaction force per unit length as $H_T(x,t)=P_T\delta(x-x_T)$. We assume the modal dissipation force per unit length $H_d(x,t)$ to be a product of the spatial eigenfunction function and the cantilever displacement velocity given as $H_d(x,t)=-P_d Y_n(x)(d\eta_{cn}/dt)$. The coefficient $B_n(t)$ is then obtained from Eq. (6) as $B_n(t)=P_c e^{i\omega_c t}Y_n(x_c)+P_T Y_n(x_T)-[P_d\int Y_n(x)dx](d\eta_{cn}/dt)$, where the integration in the last term is taken over the range $x=0$ to $x=L$. Substituting Eqs. (2) and (4) into Eq. (1) and collecting terms, we find that the dynamics for each mode n must independently satisfy the relation

$$\rho_B A_B Y_n(x)\frac{d^2\eta_{cn}(t)}{dt^2} + E_B I\frac{d^4 Y_n(x)}{dx^4}\eta_{cn} = P_c e^{i\omega_c t} Y_n(x_c) Y_n(x) + P_T Y_n(x_T) Y_n(x) + \left[P_d\int_0^L Y_n(x)dx\right]\frac{d\eta_{cn}}{dt}. \tag{7}$$

From Eq. (3) we write $d^4Y_n/dx^4=q_n^4Y_n$. Using this relation and the dispersion relation between q_n and ω_n, we obtain that the coefficient of η_{cn} in Eq. (7) is given by $E_BI(d^4Y_n/dx^4)=\omega_n^2\rho_BA_B$. Multiplying Eq. (7) by $Y_m(x)$ and integrating from $x=0$ to $x=L$, we obtain

$$m_c\ddot{\eta}_{cn}+\gamma_c\dot{\eta}_{cn}+k_{cn}\eta_{cn}=F_ce^{i\omega_ct}+F, \tag{8}$$

where the overdot denotes derivative with respect to time, $m_c=\rho_BA_BL$ is the total mass of the cantilever, and $F_c=P_BLY_n(x_c)$. The tip-sample interaction force F is defined by $F=P_TLY_n(x_T)$ and the cantilever stiffness constant k_{cn} is defined by $k_{cn}=m_c\omega_n^2$. The damping coefficient γ_c of the cantilever is defined as $\gamma_c=P_dL\int Y_n(x)dx$. Note that, with regard to the coupled system response, for a given mode n the effective magnitudes of the driving term F_c and the interaction force F are dependent via $Y_n(x_c)$ and $Y_n(x_T)$, respectively, on the positions x_c and x_T at which the forces are applied. The damping factor, in contrast, results from a more general dependence on x via the integral of $Y_n(x)$ over the range zero to L. If the excitation force per unit length is a distributed force over the cantilever surface rather than at a point, then the resulting calculation for F_c would involve an integral over $Y_n(x)$ as obtained for the damping coefficient.

The interaction force F in Eq. (8) is derived without regard to the cantilever tip-sample surface separation distance z. Realistically, the magnitude of F is quite dependent on the separation distance. In particular, various parameters derived from the force-separation curve play an essential role in the response of the cantilever to all driving forces. We further consider that the interaction force not only involves the cantilever at the tip position x_T but also some elemental volume of material at the sample surface. To maintain equilibrium, it is appropriate to view the elemental volume of sample surface as a mass element m_s (active mass) that, in addition to the interaction force, is subjected to a linear restoring force from material in the remainder of the sample. We assume that the restoring force per unit displacement of m_s in the direction z toward the cantilever tip is described by a sample stiffness constant k_s. The interaction force F between the cantilever tip and the mass element m_s is in general a nonlinear function of the cantilever tip-sample surface separation distance z. Since the force $F(z)$ is common to the cantilever tip and the sample surface element, the cantilever and the sample form a coupled dynamical system. We thus consider the cantilever and the sample as independent dynamical systems coupled by their common interaction force $F(z)$—a situation often encountered in the physics literature.[29–31]

Figure 1 provides a schematic representation of the various elements of the coupled system. The dynamical equations expressing the responses of the cantilever and the sample surface to all driving and damping forces may be written for each mode n of the coupled system as

$$m_c\ddot{\eta}_{cn}+\gamma_c\dot{\eta}_{cn}+k_{cn}\eta_{cn}=F(z)+F_c\cos\omega_ct, \tag{9}$$

$$m_s\ddot{\eta}_{sn}+\gamma_s\dot{\eta}_{sn}+k_s\eta_{sn}=F(z)+F_s\cos(\omega_st+\theta), \tag{10}$$

where η_{cn} (positive down) is the cantilever tip displacement for mode n, η_{sn} (positive up) is the sample surface displacement for mode n, ω_c is the angular frequency of the cantilever oscillations, ω_s is the angular frequency of the sample surface vibrations, γ_c is the damping coefficient for the cantilever, γ_s is the damping coefficient for the sample surface, F_c is the magnitude of the cantilever driving force, and F_s is the magnitude of the sample driving force that we assume here to result from an incident ultrasonic wave generated at the opposite surface of the sample. The factor θ is a phase contribution resulting from the propagation of the ultrasonic wave through the sample material.

Equations (9) and (10) are coupled equations representing the cantilever tip-sample surface dynamics resulting from the nonlinear interaction forces. The equations govern the cantilever and surface displacements η_{cn} and η_{sn}, respectively, at $x=x_T$. In a realistic AFM measurement of the cantilever response to the driving forces, the measurement point is not generally at $x=x_T$, but at the point $x=x_L$ at which the laser beam of the AFM optical detector system strikes the cantilever surface. The cantilever response at $x=x_l$ is found from Eq. (2) to be

$$y(x_L,t)=\eta_c(t)=\sum_{n=1}^{\infty}Y_n(x_L)\eta_{cn}(t). \tag{11}$$

We have shown previously[9] that for an acoustic wave propagating through a sample of thickness $a/2$ with phase velocity c and wave number k, containing an embedded feature of thickness $d/2$ for which the phase velocity is c_d, the total phase contribution θ at the sample surface opposite that of the transducer is given by

$$\theta=-(\chi+\Delta\chi), \tag{12}$$

where

$$\chi=\frac{ka}{2}+\tan^{-1}\frac{\sin ka}{e^{\alpha a}-\cos ka}, \tag{13}$$

$$\Delta\chi=-\psi\left[\frac{1}{2}+\frac{e^{\alpha a}\cos ka-1}{(e^{\alpha a}-\cos ka)^2+\sin^2 ka}\right], \tag{14}$$

and

$$\psi=kd\frac{(c_d-c)}{c_d}. \tag{15}$$

The factor $-\chi$ is the contribution to the phase from the featureless bulk material and $-\Delta\chi$ is the contribution from a phase variation due to the embedded feature.

A typical nonlinear interaction force $F(z)$ is shown schematically in Fig. 2 plotted as a function of cantilever tip-sample surface separation distance z. The interaction force results from a number of possible fundamental mechanisms including electrostatic forces, van der Waals forces, interatomic repulsive (e.g., Born–Mayer) potentials, and Casimir forces.[32–37] It is also influenced by chemical potentials as well as hydroxyl bonds resulting from atmospheric moisture accumulation on the cantilever tip and sample surface.[38]

We note from Fig. 1 that for a given mode n, $z=z_0-(\eta_{cn}+\eta_{sn})$. We use this relationship in a power series expansion of $F(z)$ about z_0 to obtain

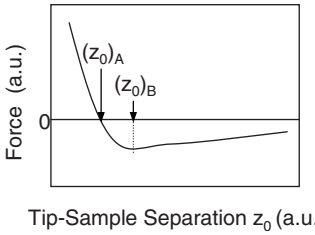

FIG. 2. Schematic of interaction force as a function of the separation distance between cantilever tip and sample surface.

$$F(z) = F(z_0) + F'(z_0)(z - z_0) + \tfrac{1}{2}F''(z_0)(z - z_0)^2 + \cdots$$
$$= F(z_0) - F'(z_0)(\eta_{cn} + \eta_{sn}) + \tfrac{1}{2}F''(z_0)(\eta_{cn} + \eta_{sn})^2 + \cdots, \quad (16)$$

where the prime denotes derivative with respect to z. Substitution of Eq. (16) into Eqs. (9) and (10) gives

$$m_c\ddot{\eta}_{cn} + \gamma_c\dot{\eta}_{cn} + [k_{cn} + F'(z_0)]\eta_{cn} + F'(z_0)\eta_{sn} = F(z_0) + F_c\cos\omega_c t + \frac{1}{2}F''(z_0)(\eta_{cn} + \eta_{sn})^2 + \cdots, \quad (17)$$

$$m_s\ddot{\eta}_{sn} + \gamma_s\dot{\eta}_{sn} + [k_s + F'(z_0)]\eta_{sn} + F'(z_0)\eta_{cn} = F(z_0) + F_s\cos(\omega_s t + \theta) + \frac{1}{2}F''(z_0)(\eta_{cn} + \eta_{sn})^2 + \cdots. \quad (18)$$

It is of interest to note that Eqs. (17) and (18) were obtained assuming that the cantilever is a rectangular beam of constant cross section. Such a restriction is not necessary, since the mathematical procedure leading to Eqs. (17) and (18) is based on the assumption that the general displacement of the cantilever can be expanded in terms of a set of eigenfunctions that form an orthogonal basis set for the problem. For the beam cantilever, the eigenfunctions are $Y_n(x)$. For some other cantilever shape, a different orthogonal basis set of eigenfunctions would be appropriate. However, the mathematical procedure used here would lead again to Eqs. (17) and (18) with values of the coefficients appropriate to the different cantilever geometry.

B. Solution to the general dynamical equations

We solve the coupled nonlinear equations (17) and (18) for the steady-state solution by writing the coupled equations in matrix form and using an iteration procedure commonly employed in the physics literature[39–41] to solve the matrix expression. The first iteration involves solving the equations for which the nonlinear terms are neglected. The second iteration is obtained by substituting the first iterative solution into the nonlinear terms of Eqs. (17) and (18) and solving the resulting equations. The procedure provides solutions both for the cantilever tip and the sample surface displacements. Since the procedure is much too lengthy to reproduce here in full detail, only the salient features of the procedure leading to the steady-state solution for the cantilever displacement $\eta_c = \Sigma Y_n \eta_{cn}$ are given. We begin by writing

$$\eta_{cn} = \varepsilon_{cn} + \xi_{cn} + \zeta_{cn} \quad (19)$$

and

$$\eta_{sn} = \varepsilon_{sn} + \xi_{sn} + \zeta_{sn}, \quad (20)$$

where ε_{cn} and ξ_{cn} represent the first iteration (i.e., linear) static and oscillatory solutions, respectively, for the nth mode cantilever displacement, ζ_{cn} represents the second iteration (i.e., nonlinear) solution for the nth mode cantilever displacement, and ε_{sn},ξ_{sn}, and ζ_{sn} are the corresponding first and second iteration nth mode displacements for the sample surface.

1. First iterative solution

The first iterative solution is obtained by linearizing Eqs. (17) and (18), writing the resulting expression in matrix form, and solving the matrix expression assuming sinusoidal driving terms $F_c e^{i\omega_c t}$ and $F_s e^{i\omega_s t}$ for the cantilever and sample surface, respectively. The first iteration yields a static solution ε_{cn} and an oscillatory solution ξ_{cn} for the cantilever. The static solution is given by

$$\varepsilon_{cn} = \frac{k_s F(z_0)}{k_{cn}k_s + F'(z_0)(k_{cn} + k_s)}. \quad (21)$$

The first iterative oscillatory solution is given by

$$\xi_{cn} = Q_{cc}\cos(\omega_c t + \alpha_{cc} - \phi_{cc}) + Q_{cs}\cos(\omega_s t - \phi_{ss} + \theta), \quad (22)$$

where

$$\phi_{cc} = \tan^{-1}\frac{\omega_c(\gamma_s k_{cn} + \gamma_c k_s) - \omega_c^3(\gamma_s m_c + \gamma_c m_s) + F'(z_0)\omega_c(\gamma_s + \gamma_c)}{k_{cn}k_s + m_s m_c\omega_c^4 - \omega_c^2(m_s k_{cn} + m_c k_s + \gamma_c\gamma_s) + F'(z_0)(k_{cn} + k_s - m_s\omega_c^2 - m_c\omega_c^2)}, \quad (23)$$

$$\phi_{ss} = \tan^{-1}\frac{\omega_s(\gamma_s k_{cn} + \gamma_c k_s) - \omega_s^3(\gamma_s m_c + \gamma_c m_s) + F'(z_0)\omega_s(\gamma_s + \gamma_c)}{k_{cn}k_s + m_s m_c\omega_s^4 - \omega_s^2(m_s k_{cn} + m_c k_s + \gamma_c\gamma_s) + F'(z_0)(k_{cn} + k_s - m_s\omega_s^2 - m_c\omega_s^2)}, \quad (24)$$

$$Q_{cc} = F_c\{[k_s + F'(z_0) - m_s\omega_c^2]^2 + \gamma_s^2\omega_c^2\}^{1/2}\{[k_{cn}k_s + m_s m_c\omega_c^4 - \omega_c^2(m_s k_{cn} + m_c k_s + \gamma_c\gamma_s) + F'(z_0)(k_{cn} + k_s - m_s\omega_c^2 - m_c\omega_c^2)]^2 + [\omega_c(\gamma_s k_{cn} + \gamma_c k_s) - \omega_c^3(\gamma_s m_c + \gamma_c m_s) + F'(z_0)\omega_c(\gamma_s + \gamma_c)]^2\}^{-1/2}, \quad (25)$$

and

$$Q_{cs} = -F_s F'(z_0)\{[k_{cn}k_s + m_s m_c \omega_s^4 - \omega_s^2(m_s k_{cn} + m_c k_s + \gamma_c \gamma_s) + F'(z_0)(k_{cn} + k_s - m_s\omega_s^2 - m_c\omega_s^2)]^2 + [\omega_s(\gamma_s k_{cn} + \gamma_c k_s) - \omega_s^3(\gamma_s m_c + \gamma_c m_s) + F'(z_0)\omega_s(\gamma_s + \gamma_c)]^2\}^{-1/2}. \quad (26)$$

2. Second iterative solution

The second iterative solution ζ_{cn} for each mode n of the cantilever is considerably more complicated, since it contains not only sum-frequency, difference-frequency, and harmonic-frequency components, but linear and static components as well. The second iterative solution ζ_{cn} is thus written as

$$\zeta_{cn} = \zeta_{cn,stat} + \zeta_{cn,lin} + \zeta_{cn,diff} + \zeta_{cn,sum} + \zeta_{cn,harm}, \quad (27)$$

where $\zeta_{cn,stat}$ is a static or "dc" contribution generated by the nonlinear tip-surface interaction, $\zeta_{cn,lin}$ is a generated linear oscillatory contribution, $\zeta_{cn,diff}$ is a generated difference-frequency contribution resulting from the nonlinear mixing of the cantilever and sample oscillations, $\zeta_{cn,sum}$ is a generated sum-frequency contribution resulting from the nonlinear mixing of the cantilever and sample oscillations, and $\zeta_{cn,harm}$ are generated harmonic contributions.

Generally, the cantilever responds with decreasing displacement amplitudes as the drive frequency is increased above the fundamental resonance (for some cantilevers the second resonance mode has the largest amplitude), even when driven at higher modal frequencies. Thus, acoustic atomic force microscopy methods do not generally utilize harmonic- or sum-frequency signals. For expediency, such signals from the second iteration will not be considered here. Only the static, linear, and difference-frequency terms from the second iteration solution are relevant to the most commonly used A-AFM modalities.

The static contribution generated by the nonlinear interaction force is obtained to be

$$\zeta_{cn,stat} = \frac{1}{4}\frac{k_s F''(z_0)}{[k_{cn}k_s + F'(z_0)(k_{cn} + k_s)]}[2\varepsilon_0^2 + Q_{cc}^2 + Q_{cs}^2 + Q_{sc}^2 + Q_{ss}^2 + 2Q_{cc}Q_{sc}\cos(\alpha_{cc} - 2\phi_{cc}) + 2Q_{cs}Q_{ss}\cos\alpha_{ss}], \quad (28)$$

where

$$\varepsilon_0 = \frac{(k_{cn} + k_s)F(z_0)}{k_{cn}k_s + F'(z_0)(k_{cn} + k_s)}, \quad (29)$$

$$Q_{sc} = -F_c F'(z_0)\{[k_{cn}k_s + m_s m_c \omega_c^4 - \omega_c^2(m_s k_{cn} + m_c k_s + \gamma_c \gamma_s) + F'(z_0)(k_{cn} + k_s - m_s\omega_c^2 - m_c\omega_c^2)]^2 + [\omega_c(\gamma_s k_{cn} + \gamma_c k_s) - \omega_c^3(\gamma_s m_c + \gamma_c m_s) + F'(z_0)\omega_c(\gamma_s + \gamma_c)]^2\}^{-1/2}, \quad (30)$$

$$Q_{ss} = F_s\{[k_{cn} + F'(z_0) - m_c\omega_s^2]^2 + \gamma_c^2\omega_s^2\}^{1/2}\{[k_{cn}k_s + m_s m_c \omega_s^4 - \omega_s^2(m_s k_{cn} + m_c k_s + \gamma_c \gamma_s) + F'(z_0)(k_{cn} + k_s - m_s\omega_s^2 - m_c\omega_s^2)]^2 + [\omega_s(\gamma_s k_{cn} + \gamma_c k_s) - \omega_s^3(\gamma_s m_c + \gamma_c m_s) + F'(z_0)\omega_s(\gamma_s + \gamma_c)]^2\}^{-1/2}, \quad (31)$$

$$\alpha_{cc} = \tan^{-1}\frac{\gamma_s\omega_c}{k_s + F'(z_0) - m_s\omega_c^2}, \quad (32)$$

$$\alpha_{ss} = \tan^{-1}\frac{\gamma_c\omega_s}{k_{cn} + F'(z_0) - m_c\omega_s^2}, \quad (33)$$

and ϕ_{cc} is given by Eq. (23), Q_{cc} by Eq. (25), and Q_{cs} by Eq. (26).

The linear oscillatory contribution $\zeta_{cn,lin}$ generated by the nonlinear interaction force in the second iteration is obtained to be

$$\zeta_{cn,lin} = \frac{D_c}{R_{cc}}\varepsilon_0 F''(z_0)[Q_{cc}^2 + Q_{sc}^2 + 2Q_{cc}Q_{sc}\cos\alpha_{cc}]^{1/2} \times\cos(\omega_c t - 2\phi_{cc} + \beta_c + \mu_{cc}) + \frac{D_s}{R_{ss}}\varepsilon_0 F''(z_0)[Q_{ss}^2 + Q_{cs}^2 + 2Q_{ss}Q_{cs}\cos\alpha_{ss}]^{1/2}\cos(\omega_s t - 2\phi_{ss} + \beta_s + \mu_{ss} + \theta), \quad (34)$$

where

$$\mu_{cc} = \tan^{-1}\frac{Q_{cc}\sin\alpha_{cc}}{Q_{cc}\cos\alpha_{cc} + Q_{sc}}, \quad (35)$$

$$\mu_{ss} = \tan^{-1}\frac{Q_{ss}\sin\alpha_{ss}}{Q_{ss}\cos\alpha_{ss} + Q_{cs}}, \quad (36)$$

$$\beta_c = \tan^{-1}\frac{\gamma_s\omega_c}{k_s - m_s\omega_c^2}, \quad (37)$$

$$\beta_s = \tan^{-1}\frac{\gamma_s\omega_s}{k_s - m_s\omega_s^2}, \quad (38)$$

$$D_c = [(k_s - m_s\omega_c^2)^2 + \gamma_s^2\omega_c^2]^{1/2}, \quad (39)$$

$$D_s = [(k_s - m_s\omega_s^2)^2 + \gamma_s^2\omega_s^2]^{1/2}, \quad (40)$$

$$R_{ss} = \{[k_{cn}k_s + m_s m_c \omega_s^4 - \omega_s^2(m_s k_{cn} + m_c k_s + \gamma_c \gamma_s) + F'(z_0)(k_{cn} + k_s - m_s\omega_s^2 - m_c\omega_s^2)]^2 + [\omega_s(\gamma_s k_{cn} + \gamma_c k_s) - \omega_s^3(\gamma_s m_c + \gamma_c m_s) + F'(z_0)\omega_s(\gamma_s + \gamma_c)]^2\}^{1/2}, \quad (41)$$

and

$$R_{cc} = \{[k_{cn}k_s + m_s m_c \omega_c^4 - \omega_c^2(m_s k_{cn} + m_c k_s + \gamma_c \gamma_s) + F'(z_0) \times(k_{cn} + k_s - m_s\omega_c^2 - m_c\omega_c^2)]^2 + [\omega_c(\gamma_s k_{cn} + \gamma_c k_s) - \omega_c^3(\gamma_s m_c + \gamma_c m_s) + F'(z_0)\omega_c(\gamma_s + \gamma_c)]^2\}^{1/2}. \quad (42)$$

The difference-frequency contribution $\zeta_{cn,diff}$ generated by the nonlinear interaction force in the second iteration is obtained to be

$$\zeta_{cn,diff} = G_n \cos[(\omega_c - \omega_s)t - \phi_{cc} + \phi_{ss} + \beta_{cs} - \phi_{cs} + \Gamma - \theta], \tag{43}$$

where

$$G_n = \frac{1}{2}\frac{D_{cs}}{R_{cs}}F''(z_0)\{Q_{cc}^2Q_{cs}^2 + Q_{sc}^2Q_{ss}^2 + Q_{cc}^2Q_{ss}^2 + Q_{cs}^2Q_{sc}^2 + 2Q_{cc}Q_{cs}Q_{sc}Q_{ss}\cos(\alpha_{cc} + \alpha_{ss}) + 2Q_{cc}^2Q_{cs}Q_{ss}\cos\alpha_{ss} + 2Q_{cc}Q_{cs}^2Q_{sc}\cos\alpha_{cc} + 2Q_{sc}^2Q_{ss}Q_{cs}\cos\alpha_{ss} + 2Q_{cc}Q_{ss}Q_{cs}Q_{sc}\cos(\alpha_{cc} - \alpha_{ss})\}^{1/2}, \tag{44}$$

$$D_{cs} = \sqrt{[k_s - m_s(\omega_c - \omega_s)]^2 + \gamma_s^2(\omega_c - \omega_s)^2}, \tag{45}$$

$$R_{cs} = \sqrt{R_{cs1}^2 + R_{cs2}^2}, \tag{46}$$

$$R_{cs1} = k_{cn}k_s - m_sk_{cn}(\omega_c - \omega_s)^2 - m_ck_s(\omega_c - \omega_s)^2 + m_sm_c(\omega_c - \omega_s)^4 - \gamma_c\gamma_s(\omega_c - \omega_s)^2 + F'(z_0)[k_{cn} + k_s - m_s(\omega_c - \omega_s)^2 - m_c(\omega_c - \omega_s)^2], \tag{47}$$

$$R_{cs2} = (\omega_c - \omega_s)(\gamma_sk_c + \gamma_ck_s) - (\omega_c - \omega_s)^3(\gamma_sm_c + \gamma_cm_s) + F'(z_0)(\omega_c - \omega_s)(\gamma_s + \gamma_c), \tag{48}$$

$$\phi_{cs} = \tan^{-1}\frac{R_{cs2}}{R_{cs1}}, \tag{49}$$

$$\beta_{cs} = \tan^{-1}\frac{\gamma_s(\omega_c - \omega_s)}{k_s - m_s(\omega_c - \omega_s)^2}, \tag{50}$$

and

$$\Gamma = \tan^{-1}\frac{Q_{cc}Q_{cs}\sin\alpha_{cc} - Q_{sc}Q_{ss}\sin\alpha_{ss} + Q_{cc}Q_{ss}\sin(\alpha_{cc} - \alpha_{ss})}{Q_{cc}Q_{cs}\cos\alpha_{cc} + Q_{sc}Q_{ss}\cos\alpha_{ss} + Q_{cc}Q_{ss}\cos(\alpha_{cc} - \alpha_{ss}) + Q_{cs}Q_{sc}}. \tag{51}$$

3. Salient features of the solution set

The present derivation is based on the well-established fact that the cantilever tip-sample surface interaction force is a smooth (multiply differentiable), continuous, nonlinear function of the tip-surface separation distance as indicated in Fig. 2. Points on the curve below a certain separation distance $(z_0)_A$ in Fig. 2 correspond to a repulsive interaction force, while points above $(z_0)_A$ correspond to an attractive force. The force-separation curve has a minimum at a separation distance $(z_0)_B$ corresponding to the maximum nonlinearity of the curve and that point lies in the attractive force portion of the curve. Cantilever oscillations result in continuous oscillatory changes in the tip-surface separation distance about the quiescent tip-surface separation distance. Since the cantilever oscillations are constrained to follow the force-separation curve, the fractions of the cantilever oscillation cycle in the repulsive and attractive portions of the force-separation curve depend on the quiescent tip-surface separation distance and the amplitude of the oscillations.

The total static solution to the coupled nonlinear equations (17) and (18) for the cantilever $\eta_{cn,stat}$ is the sum of the contribution ε_{cn}, given by Eq. (21), from the first iterative solution and the contribution $\zeta_{cn,stat}$, given by Eq. (28), from the second iteration as

$$\eta_{cn,stat} = \varepsilon_{cn} + \zeta_{cn,stat}. \tag{52}$$

The total linear solution $\eta_{cn,lin}$ to Eqs. (17) and (18) is the sum of the contribution ξ_{cn} given by Eq. (22) and the contribution $\zeta_{cn,lin}$ given by Eq. (34) as

$$\eta_{cn,lin} = \xi_{cn} + \zeta_{cn,lin}. \tag{53}$$

The total difference-frequency solution $\eta_{cn,diff}$ to Eqs. (17) and (18) is simply the contribution $\zeta_{cn,diff}$ given by Eq. (43).

It is interesting to note that ε_{cn} and the component ε_0 in $\eta_{cn,stat}$ do not explicitly involve the cantilever drive amplitude F_c and the sample surface drive amplitude F_s, although other terms involving the Q factors, given by Eqs. (25), (26), (30), and (31), in $\zeta_{cn,stat}$ do involve these drive amplitudes. This means that only the contributions stemming from the nonlinearity in the cantilever tip-sample surface interaction force respond directly to variations in the drive amplitudes and, in particular, to the physical features of the material giving rise to variations in F_s. Furthermore, the magnitudes of all second iteration (i.e., nonlinear) contributions, $\zeta_{cn,stat}$, $\zeta_{cn,lin}$, and $\zeta_{cn,diff}$, are strongly dependent on the cantilever tip-sample surface quiescent separation z_0, since the value of the nonlinear stiffness constant $F''(z_0)$ that dominates these contributions is highly sensitive to z_0. Indeed, $F''(z_0)$ attains a maximum value near the bottom of the force-separation curve of Fig. 2.

For large deflections of the cantilever that may occur for sufficiently hard contact, large bending moments that produce frequency shifts in the cantilever resonance frequencies quite apart from those introduced by the interaction force stiffness constant $F'(z_0)$ may be introduced. For the assessment of $F'(z_0)$ near the bottom of the force-separation curve where $F''(z_0)$ is maximum [maximum nonlinearity regime (MNR)] and $F'(z_0)$ is relatively small, the bending moments are generally negligible and a reasonable estimate of $F'(z_0)$ can be obtained directly from differences in the engaged and

nonengaged resonance (free space) frequencies of the cantilever.

For large driving force amplitudes, nonlinear modes of oscillation may be generated in the cantilever. Nonlinear tip-surface interactions are also known to excite nonlinear (anharmonic) cantilever modes.[23,26] It is assumed that the nonlinear modes can be described in terms of a set of orthogonal eigenfunctions $Z_n(x)$ [generally different from but also orthogonal to $Y_n(x)$] describing the nonlinearities of the unforced cantilever. In such case, the nonlinear vibrational characteristics of the cantilever may also be included in the general cantilever response in a manner similar to that given above for the linear modes. The nonlinear modes are thus formally included in the present model by extending the set of eigenvalues k_{cn}, hence eigenvectors spanning the function space, to allow for nonlinear eigenmodes. This requires no additional formal analysis in the present model. All eigenvalues (including those from nonlinear modes) are ascertained in the present model from experimental measurements.

We point out that for AM-AFM operation the cantilever oscillations are known to be bistable with the particular mode of oscillation being determined by the initial conditions that includes the tip-surface separation distance.[26] Unless some extraneous perturbation changes the mode of oscillation, the cantilever continues to oscillate in a given bistable mode for a given set of initial conditions. For large oscillation amplitudes, the bistability coalesces to a single stable mode.[26] In the present model, the bistable mode of cantilever oscillation is set by the value of the "effective" sample stiffness constant k_s that has one of the two values—one associated with the repulsive portion of the force-separation curve and one associated with the attractive portion (see Sec. IV A 3). The value of the effective sample stiffness constant, hence cantilever oscillation mode, must be determined experimentally in the present model. The present model thus accounts phenomenologically for the more complex oscillations in the intermittent contact mode as well as all other modes of operation considered in Sec. III.

III. APPLICATION OF MODEL TO VARIOUS ACOUSTIC ATOMIC FORCE MICROSCOPE TECHNIQUES

The equations derived in Sec. II describing the cantilever response resulting from the interaction with the nonlinear cantilever tip-sample surface forces may be used to quantify the signal generation and contrast for a number of A-AFM modalities. We shall consider the most frequently used A-AFM modalities including resonant difference-frequency atomic force ultrasonic microscopy,[9] heterodyne force microscopy,[7,8] ultrasonic force microscopy,[5,6] atomic force acoustic microscopy,[3,4] force modulation microscopy,[2] and the most commonly used amplitude modulation—atomic force microscopy (intermittent contact or tapping mode). We note in applying the above equations that for the range of frequencies generally employed in A-AFM the contribution from terms involving the mass of the sample element m_s is small compared to the remaining terms and may to an excellent approximation be neglected.

A. Resonant difference-frequency atomic force ultrasonic microscopy and heterodyne force microscopy

RDF-AFUM[9] employs an ultrasonic wave launched from the bottom of a sample, while the AFM cantilever tip engages the sample top surface. The cantilever is driven at a frequency differing from the ultrasonic frequency by one of the resonance frequencies of the engaged cantilever. It is important to note that at high drive amplitudes of the ultrasonic wave or engaged cantilever (or both) the resonance frequency generating the difference-frequency signal may correspond to one of the nonlinear oscillation modes of the cantilever. The engaged cantilever resonance frequency for the (linear or nonlinear) mode n, neglecting dissipation, is given by $m_c\omega_{cn}^2=k_{cn}+F'(z_0)k_{cn}[k_s+F'(z_0)]^{-1}$, where k_{cn} is the cantilever stiffness constant corresponding to the nth (linear or nonlinear) nonengaged (free space) resonance mode. Since $F'(z_0)$ may be positive or negative, depending on the shape of the force-separation curve, at the separation distance z_0 corresponding to maximum $F''(z_0)$, the resonance frequency of the cantilever when engaged at this value of z_0 may be larger or smaller, respectively, than the resonance frequency when not engaged. The nonlinear mixing of the oscillating cantilever and the ultrasonic wave in the region defined by the cantilever tip-sample surface interaction force generates difference-frequency oscillations at the engaged cantilever resonance.

Variations in the amplitude and phase of the bulk wave due to the presence of subsurface nano/microstructures as well as variations in near-surface material parameters affect the amplitude and phase of the difference-frequency signal. These variations are used to create spatial mappings generated by subsurface and near-surface structures. HFM[7,8] also utilizes difference-frequency signals generated by the nonlinear mixing in the cantilever tip-sample surface interaction region. In this technique, no special advantage is taken of cantilever resonances and the difference-frequency utilized is generally well below that of the cantilever resonance.

In both RDF-AFUM and HFM, the cantilever difference-frequency response is obtained from the nonlinear mixing in the region defined by the tip-surface interaction force. The interaction force varies nonlinearly with the tip-surface separation distance. The deflection of the cantilever obtained in calibration plots is related to this force; for small slopes of the deflection versus separation distance, the interaction force and cantilever deflection curves are approximately related via a constant of proportionality. The maximum difference-frequency signal amplitude occurs when the quiescent deflection of the cantilever is near the bottom of the force curve. There the maximum change in the slope of the force versus separation curve (hence maximum interaction force nonlinearity) occurs. We shall call this region of operation the maximum nonlinearity regime.

The dominant term or terms for the cantilever difference-frequency displacement in Eqs. (11) and (19) depend on the values of k_{cn} for the free modes of cantilever oscillation, $\omega_c-\omega_s$, and the value of $F'(z_0)$ obtained at the separation distance $z_0=(z_0)_B$ at which the maximum difference-frequency signal occurs. We designate the nonengaged linear or nonlinear mode n for which the difference-frequency en-

gaged resonance occurs as $n=p$. The dominant difference-frequency component in Eqs. (11) and (19) is thus $\eta_{cp}=\eta_{cp,diff}=\zeta_{cp,diff}$ and is given by Eq. (43) for $n=p$ as

$$\zeta_{cp,diff}=G_p\cos[(\omega_c-\omega_s)t-\phi_{cc}+\phi_{ss}+\beta_{cs}-\phi_{cs}+\Gamma-\theta], \tag{54}$$

where G_p, given by Eq. (44), and the phase terms in Eq. (54) are obtained from Eqs. (23)–(26), (29)–(33), and (45)–(51). It is important to point out in considering these equations that while the difference-frequency resonance frequency $(\omega_c-\omega_s)$ in RDF-AFUM is usually set to correspond to the lowest resonance mode of the engaged cantilever (although a higher modal resonance could be used), the cantilever driving frequency ω_c and ultrasonic frequency ω_s generally are set near (but not necessary equal to) higher resonance modes $n=q$ and $n=r$, respectively, of the engaged cantilever. For relatively small difference frequencies, it may occur that $q=r$. Thus, the cantilever stiffness constant k_{cn} is appropriately given as k_{cp} when involving the difference-frequency terms in Eqs. (23)–(26), (29)–(33), and (45)–(51), the stiffness constant k_{cq} when involving the cantilever drive frequency ω_c at or near the frequency of the qth cantilever resonance mode, and k_{cr} when involving the ultrasonic frequency ω_s at or near the frequency of the rth cantilever resonance mode. If ω_c and ω_s are not set at or near a resonance modal frequency of the engaged cantilever, then it may be necessary to include more than one term in Eqs. (11) and (19) corresponding to various values of q and r.

It is seen from Eq. (44) that for a given value of $(\omega_c-\omega_s)$ the maximum value of $\zeta_{cp,diff}$ ideally occurs for a value of z_0 such that $F''(z_0)$ is maximized. It is important to note, however, that $F'(z_0)$, while relatively small in magnitude compared to that of the hard contact regime, is generally not equal to zero at that point. Strictly, the values of $F''(z_0)$ and $F'(z_0)$ for a given z_0 are each dependent on the exact functional form of $F(z_0)$. A functional form for $F(z_0)$ sufficiently quantitative to quantify $F''(z_0)$ and $F'(z_0)$ is not typically available. However, experimental curves for $F(z_0)$ can be obtained and compared to the experimental curves of $\zeta_{cp,diff}$ plotted as a function of z_0. An examination of Eq. (44) suggests that a more exact approach to maximizing $\zeta_{cp,diff}$ would be not only to vary z_0 but also to vary slightly the difference frequency from the free space resonance condition until an optimal setting for both z_0 and the difference frequency is achieved.

The equations for G_p and the phase terms in Eq. (54) may be obtained from Eqs. (23)–(26), (29)–(33), and (45)–(51), where the terms involving the sample mass m_s may be dropped to an excellent approximation. For ultrasonic wave and cantilever drive frequencies in the low megahertz range, we obtain, setting $\Delta\omega=(\omega_c-\omega_s)$, that

$$\beta_{cs}\approx\tan^{-1}\frac{\gamma_s(\Delta\omega)}{k_s}, \tag{55}$$

$$\phi_{cs}\approx\tan^{-1}\frac{(\gamma_c k_s+\gamma_s k_{cp})(\Delta\omega)-\gamma_s m_c(\Delta\omega)^3+F'(z_0)(\gamma_c+\gamma_s)(\Delta\omega)}{k_{cp}k_s-(m_c k_s+\gamma_c\gamma_s)(\Delta\omega)^2+F'(z_0)[k_{cp}+k_s-m_c(\Delta\omega)^2]}, \tag{56}$$

$$\phi_{cc}\approx\tan^{-1}\frac{(\gamma_c k_s+\gamma_s k_{cq})\omega_c-\gamma_s m_c\omega_c^3+F'(z_0)(\gamma_c+\gamma_s)\omega_c}{k_{cq}k_s-(m_c k_s+\gamma_c\gamma_s)\omega_c^2+F'(z_0)(k_{cq}+k_s-m_c\omega_c^2)}, \tag{57}$$

$$\phi_{ss}\approx\tan^{-1}\frac{(\gamma_c k_s+\gamma_s k_{cr})\omega_s-\gamma_s m_c\omega_s^3+F'(z_0)(\gamma_c+\gamma_s)\omega_s}{k_{cr}k_s-(m_c k_s+\gamma_c\gamma_s)\omega_s^2+F'(z_0)(k_{cr}+k_s-m_c\omega_s^2)}, \tag{58}$$

and G_p is given by Eq. (44) where

$$\frac{D_{cs}}{R_{cs}}\approx([k_s^2+\gamma_s^2(\Delta\omega)^2]^{1/2}\{k_{cp}k_s-(\Delta\omega)^2(m_c k_s+\gamma_c\gamma_s)+F'(z_0)\times[k_{cp}+k_s-m_c(\Delta\omega)^2]\}^2+[(\Delta\omega)(\gamma_s k_{cp}+\gamma_c k_s)-(\Delta\omega)^3\gamma_s m_c+F'(z_0)\omega_c(\gamma_s+\gamma_c)]^2)^{-1/2}, \tag{59}$$

$$Q_{cc}\approx F_c\{[k_s+F'(z_0)]^2+\gamma_s^2\omega_c^2\}^{1/2}\{[k_{cq}k_s-\omega_c^2(m_c k_s+\gamma_c\gamma_s)+F'(z_0)(k_{cq}+k_s-m_c\omega_c^2)]^2+[\omega_c(\gamma_s k_{cq}+\gamma_c k_s)-\omega_c^3\gamma_s m_c+F'(z_0)\omega_c(\gamma_s+\gamma_c)]^2\}^{-1/2}, \tag{60}$$

$$Q_{ss}\approx F_s\{[k_s+F'(z_0)]^2+\gamma_s^2\omega_s^2\}^{1/2}\{[k_{cr}k_s-\omega_s^2(m_c k_s+\gamma_c\gamma_s)+F'(z_0)(k_{cr}+k_s-m_c\omega_s^2)]^2+[\omega_s(\gamma_s k_{cr}+\gamma_c k_s)-\omega_s^3\gamma_s m_c+F'(z_0)\omega_c(\gamma_s+\gamma_c)]^2\}^{-1/2}, \tag{61}$$

$$Q_{cs}\approx -F_s F'(z_0)\{[k_{cr}k_s-\omega_s^2(m_c k_s+\gamma_c\gamma_s)+F'(z_0)(k_{cr}+k_s-m_c\omega_s^2)]^2+[\omega_s(\gamma_s k_{cr}+\gamma_c k_s)-\omega_s^3\gamma_s m_c+F'(z_0)\omega_s(\gamma_s+\gamma_c)]^2\}^{-1/2}, \tag{62}$$

and

$$Q_{sc}\approx -F_c F'(z_0)\{[k_{cq}k_s-\omega_c^2(m_c k_s+\gamma_c\gamma_s)+F'(z_0)(k_{cq}+k_s-m_c\omega_c^2)]^2+[\omega_c(\gamma_s k_{cq}+\gamma_c k_s)-\omega_c^3\gamma_s m_c+F'(z_0)\omega_c(\gamma_s+\gamma_c)]^2\}^{-1/2}. \tag{63}$$

The phase term Γ in Eq. (54) is given by Eq. (51) and is quite complicated. However, advantage can be taken of the fact that k_s is generally large compared to other terms in the numerators of Q_{cc}, Q_{ss}, Q_{cs}, and Q_{sc}; the denominators of these terms are very roughly all equal. Hence, the magni-

tudes of Q_{cc} and Q_{ss} are usually large compared to those of Q_{cs} and Q_{sc}. The terms involving the $Q_{cc}Q_{ss}$ thus dominate in Eq. (51) and we may approximate Γ as

$$\Gamma \approx \alpha_{cc} - \alpha_{ss} = \tan^{-1}\frac{\gamma_s\omega_c}{k_s + F'(z_0)} - \tan^{-1}\frac{\gamma_c\omega_s}{k_{cr} + F'(z_0) - m_c\omega_s^2}, \tag{64}$$

where α_{cc} and α_{ss} are obtained from Eqs. (32) and (33), respectively. To the same extent that Γ may be approximated by Eq. (64), we may approximate G_p as

$$G_p \approx \frac{F''(z_0)}{2}\frac{D_{cs}}{R_{cs}}Q_{cc}Q_{ss}. \tag{65}$$

It is seen from Eqs. (54) and (65) that both the amplitude and phase of the difference-frequency signal $\zeta_{cp,diff}$ are dependent on F_s, F_c, k_s, k_c, γ_s, and γ_c in addition to ω_c and ω_s. Since from the Hertzian theory k_s is dependent on the Young modulus of the material, the dependence of $\zeta_{cp,diff}$ on γ_s and k_s means that scans of the sample contain information about the elastic stiffness of the sample as well as information about surface damping, hence, the viscoelastic properties of the sample surface. Subsurface features of the sample are obtained via the dependence of the difference-frequency signal amplitude on F_s and via the dependence of the difference-frequency phase signal on θ, since both F_s and θ vary as the result of ultrasonic wave scattering from subsurface features. The signal response for HFM is generally given by the same equations as those for RDF-AFUM except that a single mode p may not necessarily dominate the signal, if the difference frequency is above the lowest resonance frequency of the engaged cantilever. A sum of the largest modal contributions is thus calculated for HFM to obtain the signal output. However, the difference frequency in HFM generally is set well below the lowest modal frequency of the engaged cantilever. In this case, the appropriate equations are identical to those of RDF-AFUM with p equal to the lowest modal frequency of the engaged cantilever.

B. Ultrasonic force microscopy

In ultrasonic force microscopy[5,6] (UFM), the cantilever drive frequency ω_c and drive amplitude F_c are zero; the surface drive amplitude F_s and the drive frequency ω_s of the wave generated by the transducer at the bottom of the sample are nonzero. UFM can be operated at very large frequencies, even in the gigahertz range. Although the vibrational response of the cantilever is certainly quite small at such frequencies, operation at a tip-surface separation distance z_0 corresponding to the nonlinear regime of the force-separation curve, where $F''(z_0)$ is maximum, will produce a detectable static or dc signal from the interaction nonlinearity. The generated static signal is called the ultrasonic force.[7]

The nonlinear force-separation interaction results in a static displacement of the cantilever $\eta_{c,stat}$ given as

$$\eta_{c,stat} = \sum_p Y_p(x_L)\,\eta_{cp,stat} + \sum_m Z_m(x_L)\,\eta_{cm,stat}, \tag{66}$$

where $\eta_{cn,stat}$ $(n=p,m)$ is the contribution from mode n (linear or nonlinear) given by

$$\eta_{cn,stat} = \varepsilon_{cn} + \zeta_{cn,stat} \tag{67}$$

and ε_{cn} and $\zeta_{cn,stat}$ are given by Eqs. (21) and (28), respectively. The terms in Eq. (28) involving Q_{cc} and Q_{sc} are zero, since F_c is zero for UFM. We assume operation of the UFM in the nonlinear regime of the force curve where $F''(z_0)$ is maximized and $F'(z_0)$ is relatively small. We approximate the nonzero terms Q_{ss} and Q_{cs} in Eq. (28) by Eqs. (61) and (62), where k_{cq} is replaced with k_{cn}. We obtain

$$\eta_{cn,stat} = \frac{k_s}{k_{cn}k_s + F'(z_0)(k_{cn}+k_s)}\left\{F(z_0) + \frac{F''(z_0)}{4}[2\varepsilon_0^2 + Q_{cs}^2 + Q_{ss}^2 + 2Q_{cs}Q_{ss}\cos\alpha_{ss}]\right\}, \tag{68}$$

where ε_0 is given by Eq. (29) and α_{ss} is given by Eq. (33). To the extent that Q_{ss} is much larger than Q_{cs} because of the occurrence of k_s and $\gamma_s\omega_s$ in the numerator of Q_{ss}, Eq. (68) may be simplified by dropping the terms involving Q_{cs}.

Equation (66) admits all cantilever modes as contributors to the magnitude of the UFM signal. However, Eq. (68) shows that the contribution to $\eta_{c,stat}$ for a given mode n is dependent on k_{cn} such that for both the ultrasonic and nonoscillatory contributions to Eq. (68) an increase in k_{cn} results in a decrease in the magnitude of the contributions for that mode. Since k_{cn} increases in magnitude with increasing n, the contribution to $\eta_{c,stat}$ from a given mode generally decreases with increasing mode number for both the ultrasonic and nonoscillatory components of $\eta_{cn,stat}$, although the exact relationship is highly dependent on the values of γ_c, γ_s, k_s, m_c, and ω_s that appear in Eq. (68).

The dominant contributions from the second term on the right-hand side of Eq. (68) for a given ultrasonic drive frequency ω_s occur for those cantilever modes such that $m_c\omega_s^2$ has a value near $m_c\omega_{cn}^2 = k_{cn} + F'(z_0)k_{cn}[k_s + F'(z_0)]^{-1}$. In contrast, the first term on the right-hand side of Eq. (68) and the component of the second term involving ε_0 are independent of frequency and thus make the major contributions when the ultrasonic drive frequencies are in the gigahertz range. These terms predict that a static signal exists even without the presence of an ultrasonic wave propagating through the sample and results directly from the interaction of the cantilever with the sample surface via the interaction force.

It is seen from Eq. (68) that $\eta_{cn,stat}$ is dependent on both F_s and k_s. This means that scans of the sample contain information about the elastic stiffness of the sample through k_s as well as information about subsurface features via the dependence of the amplitude on F_s. The dependence on γ_s means that UFM is sensitive to the viscous properties at the sample surface as well.

C. Atomic force acoustic microscopy and force modulation microscopy

Both for AFAM[3,4] and FMM,[2] the cantilever drive amplitude and frequency are zero. As in UFM, the surface drive amplitude and the frequency ω_s are nonzero. However, unlike UFM, the surface drive frequency is limited to a range of frequencies that produces measurable displacement ampli-

tudes of cantilever oscillation. In contrast to UFM, the tip-surface interaction distance is set to operate in hard contact, the "linear detection regime" of operation, where z_0 is small, $F(z_0)$ is repulsive, $F'(z_0)$ is large and negative, and $F''(z_0)$ is negligible. In the linear detection regime, no difference frequency or harmonically generated signal is detectable, since for hard contact $F''(z_0)$ is effectively zero. The cantilever displacement amplitude $\eta_{cn,lin}$ corresponding to the nth mode is then obtained from Eq. (53) as $\eta_{cn,lin}=\varepsilon_{cn}+\zeta_{cn,lin}$. The contribution $\zeta_{cn,lin}$ resulting from the nonlinearity is given by Eq. (34) and is seen to be zero, since $F''(z_0)$ is effectively zero in the linear detection regime. The remaining contribution ε_{cn} to the cantilever displacement amplitude is given by Eq. (22). We may approximate ε_{cn}, hence $\eta_{cn,lin}$, in the low megahertz range of frequencies as

$$\eta_{cn,lin} \approx \varepsilon_{cn} \approx Q_{cs} \cos(\omega_s t - \phi_{ss} + \theta), \tag{69}$$

where Q_{cs} is given by Eq. (62), ϕ_{ss} by Eq. (58), and θ by Eq. (12).

Note that both Q_{cs} and ϕ_{ss} depend on the magnitude of $F'(z_0)$. For sufficiently hard contact, $F'(z_0)$ becomes very large and negative and may dominate the terms in Eq. (69). Under such conditions, we obtain

$$Q_{cs} \approx -F_s\{(k_{cn}+k_s-m_c\omega_s^2)^2+(\gamma_c+\gamma_s)^2\omega_s^2\}^{-1/2} \tag{70}$$

and

$$\phi_{ss} \approx \tan^{-1}\frac{(\gamma_c+\gamma_s)\omega_s}{k_{cn}+k_s-m_c\omega_s^2}. \tag{71}$$

Equations (69)–(71) show that both the amplitude and phase of the cantilever oscillations depend on k_{cn}, k_s, γ_c, γ_s, and ω_s. For AFAM driving frequencies ω_s near a cantilever resonance mode n, determined by $m_c\omega_{cn}^2=k_{cn}+F'(z_0)k_{cn}[k_s+F'(z_0)]^{-1}$, the signal amplitude is large and the cantilever displacement is dominated by that mode. For FMM, ω_s is much smaller than $\sqrt{k_{c1}/m_c}$, the fundamental cantilever free resonance frequency.

D. Amplitude modulation–atomic force microscopy

The AM-AFM mode (also called intermittent contact mode or tapping mode) is a standard feature on many atomic force microscopes for which the cantilever is driven in oscillation, but no surface oscillations resulting from bulk ultrasonic waves are generated (i.e., F_s and ω_s are zero). Thus, AM-AFM cannot be used to image subsurface features, but interesting surface properties and features can be imaged. Since AM-AFM can be used in both hard contact and maximum nonlinearity regimes (i.e., the linear and maximally nonlinear regimes, respectively, of the force-separation curve), the cantilever displacement $\eta_{cn,lin}$ for mode n is given most generally as

$$\eta_{cn.lin} = \xi_{cn} + \zeta_{cn,lin}, \tag{72}$$

where ξ_{cn} is given by Eq. (22) with the term involving Q_{cs} set equal to zero and $\zeta_{cn,lin}$ is given by Eq. (34) with all terms involving Q_{cs} and Q_{ss} set equal to zero.

For the maximum nonlinearity regime, the expression for $\eta_{cn,lin}$ is

$$\eta_{cn,lin} = H\cos(\omega_c t - \phi_{cc} + \Lambda), \tag{73}$$

where

$$\Lambda = \tan^{-1}\frac{\sin(\beta_c+\mu_{cc}-\phi_{cc}-\alpha_{cc})}{\cos(\beta_c+\mu_{cc}-\phi_{cc}-\alpha_{cc})+(Q_{cc}/W)}, \tag{74}$$

$$W = \frac{D_c}{R_{cc}}\varepsilon_0 F''(z_0)(Q_{cc}^2+Q_{sc}^2+2Q_{cc}Q_{sc}\cos\alpha_{cc})^{1/2}, \tag{75}$$

and

$$H = [Q_{cc}^2+W^2+2Q_{cc}W\cos(\beta_c+\mu_{cc}-\phi_{cc}-\alpha_{cc})]^{1/2}, \tag{76}$$

where Q_{cc} is given by Eq. (60), Q_{sc} by Eq. (63), ϕ_{cc} by Eq. (57), μ_{cc} by Eq. (35), ε_0 by Eq. (29); and a_{cc}, β_c, D_c, and R_{cc}, by Eqs. (32), (37), (39), and (42), respectively, with the terms involving m_s set equal to zero.

The complexity of the cantilever response $\eta_{cn,lin}$ is greatly reduced for the hard contact regime, where $F''(z_0)$ is negligibly small and $F'(z_0)$ is very large and negative. For sufficiently hard contact, Λ and α_{cc} are approximately zero and we obtain

$$\eta_{cn,lin} \approx Q_{cc}\cos(\omega_c t - \phi_{cc}), \tag{77}$$

where

$$Q_{cc} = F_c[(k_{cn}+k_s-m_c\omega_c^2)^2+(\gamma_c+\gamma_s)^2\omega_c^2]^{-1/2} \tag{78}$$

and

$$\phi_{cc} = \tan^{-1}\frac{(\gamma_c+\gamma_s)\omega_c}{k_{cn}+k_s-m_c\omega_c^2}. \tag{79}$$

The dependence of $\eta_{cn,lin}$ on the material damping coefficient γ_s and the sample stiffness constant k_s, both for the hard contact and the maximum nonlinearity regimes, means that AM-AFM can be used to assess the viscoelastic properties of the material irrespective of the regime of operation.

IV. IMAGE CONTRAST

All the above equations, except for Eqs. (12) and (14), were derived for constant values of the cantilever and material parameters. If, in an area scan of the sample, the parameters remain constant from point to point, the image generated from the scan would be flat and featureless. We consider here that the sample stiffness constant k_s may vary from point to point on the sample surface. Since k_s is dependent on the Young modulus E, this means that E also varies from point to point. We assume that the value of the sample stiffness constant k_s' at a given point on the surface differs from the value k_s at another position as $k_s'=k_s+\Delta k_s$. For any function $f(k_s)$ having a functional dependence on k_s, a variation in k_s generates a variation in $f(k_s)$ given by $\Delta f=(df/dk_s)_0\Delta k_s$, where the subscripted zero indicates evaluation at k_s. A similar expression can be obtained for the material damping parameter γ_s, but we shall not consider such variations here.

A variation in k_s produces a variation both in the amplitude and phase of the signal generated by the cantilever tip-

sample surface interactions. The variations in amplitude and phase can be used to generate amplitude and phase images, respectively, in a surface scan of the sample. We first consider images generated by the phase variations in the signal.

A. Phase-generated images

The phase factors involved in RDF-AFUM and HFM are given from Eqs. (54), (12), and (13) to be ϕ_{cc}, ϕ_{ss}, β_{cs}, ϕ_{cs}, Γ, and χ; the phase factors involved in AFAM and FMM are, from Eq. (69), ϕ_{ss} and χ; and the phase factors involved in the AM-AFM mode are, from Eq. (73), ϕ_{cc} and Λ. Each of these phase factors is dependent on k_s and the variations in the phase factors resulting from variations in k_s are responsible for image generation when using phase detection of the A-AFM signal. The exact dependence of the phase on k_s, however, is different for hard contact and maximum nonlinearity regimes.

1. Maximum nonlinearity regime

For the maximum nonlinearity regime, the appropriate variations in the phase factors relevant to HFM and RDF-AFUM are

$$\Delta\beta_{cs} = \left(\frac{d\beta_{cs}}{dk_s}\right)_0 \Delta k_s = -\frac{\gamma_s \Delta\omega}{[k_s + F'(z_0)]^2 + \gamma_s^2(\Delta\omega)^2}\Delta k_s, \tag{80}$$

$$\Delta\phi_{cc} = -\frac{A_{cc}}{B_{cc}}\Delta k_s, \tag{81}$$

where

$$A_{cc} = [\gamma_s k_{cq}^2 + 2F'(z_0)\gamma_s k_{cq} + F'(z_0)^2(\gamma_c + \gamma_s)]\omega_c + \{\gamma_c^2\gamma_s - 2\gamma_s m_c[k_{cq} + F'(z_0)]\}\omega_c^3 + m_c^2\gamma_s\omega_c^5 \tag{82}$$

and

$$B_{cc} = \{[\gamma_c k_s + \gamma_s k_{cq} + F'(z_0)(\gamma_c + \gamma_s)]\omega_c - \gamma_s m_c\omega_c^3\}^2 + \{[k_{cq} - m_c\omega_c^2 + F'(z_0)]k_s + F'(z_0)(k_{cq} - m_c\omega_c^2) - \gamma_c\gamma_s\omega_c^2\}^2, \tag{83}$$

$$\Delta\phi_{ss} = -\frac{A_{ss}}{B_{ss}}\Delta k_s, \tag{84}$$

where

$$A_{ss} = [\gamma_s k_{cr}^2 + 2F'(z_0)\gamma_s k_{cr} + F'(z_0)^2(\gamma_c + \gamma_s)]\omega_s + \{\gamma_c^2\gamma_s - 2\gamma_s m_c[k_{cr} + F'(z_0)]\}\omega_s^3 + m_c^2\gamma_s\omega_s^5 \tag{85}$$

and

$$B_{ss} = \{[\gamma_c k_s + \gamma_s k_{cr} + F'(z_0)(\gamma_c + \gamma_s)]\omega_s - \gamma_s m_c\omega_s^3\}^2 + \{[k_{cr} - m_c\omega_s^2 + F'(z_0)]k_s + F'(z_0)(k_{cr} - m_c\omega_s^2) - \gamma_c\gamma_s\omega_s^2\}^2, \tag{86}$$

and

$$\Delta\phi_{cs} = -\frac{A_{cs}}{B_{cs}}\Delta k_s, \tag{87}$$

where

$$A_{cs} = [\gamma_s k_{cp}^2 + 2F'(z_0)\gamma_s k_{cp} + F'(z_0)^2(\gamma_c + \gamma_s)](\Delta\omega) + \{\gamma_c^2\gamma_s - 2\gamma_s m_c[k_{cp} + F'(z_0)]\}(\Delta\omega)^3 + m_c^2\gamma_s(\Delta\omega)^5 \tag{88}$$

and

$$B_{cs} = \{[\gamma_c k_s + \gamma_s k_{cp} + F'(z_0)(\gamma_c + \gamma_s)](\Delta\omega) - \gamma_s m_c(\Delta\omega)^3\}^2 + \{[k_{cp} - m_c(\Delta\omega)^2 + F'(z_0)]k_s + F'(z_0)[k_{cp} - m_c(\Delta\omega)^2] - \gamma_c\gamma_s(\Delta\omega)^2\}^2. \tag{89}$$

To the extent that $\Gamma = \alpha_{cc} - \alpha_{ss}$, as given by Eq. (60), we may write

$$\Delta\Gamma = \Delta\alpha_{cc} = -\frac{\gamma_s\omega_c}{[k_s + F'(z_0)]^2 + \gamma_s^2\omega_c^2}\Delta k_s. \tag{90}$$

The phase term $\Delta\chi$ is given by Eqs. (14) and (15).

The appropriate variations in the phase factors relevant to the AM-AFM maximum nonlinearity regime are $\Delta\alpha_{cc}$, $\Delta\phi_{cc}$, and $\Delta\Lambda$. The factor $\Delta\Lambda$ is obtained from Eq. (74) as

$$\Delta\Lambda = \frac{1 + (Q_{cc}/W)\cos(\beta_c + \mu_{cc} - \phi_{cc} - \alpha_{cc})}{[\cos(\beta_c + \mu_{cc} - \phi_{cc} - \alpha_{cc}) + (Q_{cc}/W)]^2 + \sin^2(\beta_c + \mu_{cc} - \phi_{cc} - \alpha_{cc})}(\Delta\beta_c + \Delta\mu_{cc} - \Delta\phi_{cc} - \Delta\alpha_{cc}), \tag{91}$$

where

$$\Delta\beta_c = -\frac{\gamma_s\omega_c}{k_s^2 + \gamma_s^2\omega_c^2}\Delta k_s, \tag{92}$$

$\Delta\phi_{cc}$ is given by Eq. (81), and $\Delta\mu_{cc}$ is obtained from Eq. (35). To the extent that Q_{sc} is much smaller than Q_{cc}, we get from Eq. (35) that $\Delta\mu_{cc} = \Delta\alpha_{cc}$, where $\Delta\alpha_{cc}$ is given by Eq. (90).

2. Hard contact regime

For the hard contact regime where $F'(z_0)$ is very large and negative, the relevant phase variations are obtained from Eqs. (71) and (79) as

$$\Delta\phi_{cc} = -\frac{(\gamma_c+\gamma_s)\omega_c}{(k_s+k_{cq}-m_c\omega_c^2)^2+(\gamma_c+\gamma_s)^2\omega_c^2}\Delta k_s, \quad (93)$$

and

$$\Delta\phi_{ss} = -\frac{(\gamma_c+\gamma_s)\omega_s}{(k_s+k_{cr}-m_c\omega_s^2)^2+(\gamma_c+\gamma_s)^2\omega_s^2}\Delta k_s. \quad (94)$$

Equations (93) and (94) are appropriate to AFAM and FMM modalities as well as to the AM-AFM hard contact mode of A-AFM operation. As a word of caution, the extent to which the hard contact equations apply depends on how well the approximation $F'(z_0)\to-\infty$ holds. In those cases where such an assumption is suspect, all terms in the equations for a given modality should be used.

3. Dependence on the Young modulus

Hertzian contact theory provides that the sample stiffness constant k_s is related to the Young modulus E of the sample as[14]

$$k_s = 2r_c\left(\frac{1-\nu_T^2}{E_T}+\frac{1-\nu^2}{E}\right)^{-1}, \quad (95)$$

where ν is the Poisson ratio of the sample material, E_T and ν_T are the Young modulus and Poisson ratio, respectively, of the cantilever tip, and r_c is the cantilever tip-sample surface contact radius. Hence,

$$\Delta k_s = \frac{2r_c(1-\nu^2)}{E^2}\left(\frac{1-\nu_T^2}{E_T}+\frac{1-\nu^2}{E}\right)^{-2},$$

$$\Delta E = \frac{k_s}{E}\left(\frac{1-\nu_T^2}{E_T}+\frac{1-\nu^2}{E}\right)^{-1}\frac{\Delta E}{E}. \quad (96)$$

Strictly, Eq. (95) was derived for the case of repulsive interaction forces leading to a concave elastic deformation of a flat sample surface from a contacting hard spherical object. However, we consider here that to a reasonable approximation Eqs. (95) and (96) also hold for attractive interactive forces providing that the elastic deformation of the sample surface is viewed as a convex deformation (asperity) subtending an effective contact radius r_c with the cantilever tip that is appropriately different in magnitude from that of the repulsive force case. As pointed out in Sec. II B 3 for AM-AFM operation, the cantilever oscillations are known to be bistable with the particular mode of oscillation being determined by the initial conditions that includes the tip-surface separation distance. In the present model, the bistable mode of cantilever oscillation is set by the value of the effective sample stiffness constant k_s corresponding either to the repulsive region or attractive region of the force-separation curve.

Equation (96) can be used with Eqs. (80)–(94) to ascertain the fractional variation in the Young modulus $\Delta E/E$ from measurements of the phase variation in the signal from an appropriate A-AFM modality. For the case where $E_T \gg E$, e.g., for polymeric or soft biological materials, Eq. (95) reduces to $k_s=2r_cE$ and Eq. (96) reduces to $\Delta k_s=k_s(\Delta E/E)$.

B. Amplitude-generated images

1. Resonant difference-frequency atomic force ultrasonic microscopy and heterodyne force microscopy

The amplitude G_p of the RDF-AFUM signal is given by Eq. (65) to a good approximation for most applications. The fractional variation in the signal amplitude $\Delta G_p/G_p$ resulting from variations in the sample stiffness constant k_s, hence Young modulus E, makes a considerable contribution to the image contrast when operating in the amplitude detection modality. The fractional variation in amplitude is

$$\frac{\Delta G_p}{G_p} = \frac{1}{G_p}\left(\frac{\partial G_p}{\partial k_s}\right)_0\Delta k_s = \left\{\frac{1}{Q_{ss}}\left(\frac{\partial Q_{ss}}{\partial k_s}\right)_0+\frac{1}{Q_{cc}}\left(\frac{\partial Q_{cc}}{\partial k_s}\right)_0 + \frac{R_{cs}}{D_{cs}}\left[\frac{\partial}{\partial k_s}\left(\frac{D_{cs}}{R_{cs}}\right)\right]_0\right\}\Delta k_s, \quad (97)$$

where

$$\frac{1}{Q_{ss}}\left(\frac{\partial Q_{ss}}{\partial k_s}\right)_0 = \frac{k_s+F'(z_0)}{\{[k_s+F'(z_0)]^2+c_{ss}^2\}^{1/2}} - \frac{(a_{ss}k_s+b_{ss})a_{ss}+(c_{ss}k_s+d_{ss})c_{ss}}{(a_{ss}k_s+b_{ss})^2+(c_{ss}k_s+d_{ss})^2}, \quad (98)$$

$$a_{ss} = k_{cr}-m_c\omega_s^2+F'(z_0), \quad (99)$$

$$b_{ss} = F'(z_0)(k_{cr}-m_c\omega_s^2)-\gamma_c\gamma_s\omega_s^2, \quad (100)$$

$$c_{ss} = \gamma_c\omega_s, \quad (101)$$

$$d_{ss} = \gamma_s k_{cr}\omega_s - m_c\gamma_s\omega_s^3+F'(z_0)(\gamma_c+\gamma_s); \quad (102)$$

$$\frac{1}{Q_{cc}}\left(\frac{\partial Q_{cc}}{\partial k_s}\right)_0 = \frac{k_s+F'(z_0)}{\{[k_s+F'(z_0)]^2+c_{cc}^2\}^{1/2}} - \frac{(a_{cc}k_s+b_{cc})a_{cc}+(c_{cc}k_s+d_{cc})c_{cc}}{(a_{cc}k_s+b_{cc})^2+(c_{cc}k_s+d_{cc})^2}, \quad (103)$$

$$a_{cc} = k_{cq}-m_c\omega_c^2+F'(z_0), \quad (104)$$

$$b_{cc} = F'(z_0)(k_{cq}-m_c\omega_c^2)-\gamma_c\gamma_s\omega_c^2, \quad (105)$$

$$c_{cc} = \gamma_c\omega_c, \quad (106)$$

$$d_{cc} = \gamma_s k_{cq}\omega_c - m_c\gamma_s\omega_c^3+F'(z_0)(\gamma_c+\gamma_s); \quad (107)$$

and

$$\frac{R_{cs}}{D_{cs}}\left[\frac{\partial}{\partial k_s}\left(\frac{D_{cs}}{R_{cs}}\right)\right]_0 = \frac{k_s}{(k_s^2+c_{cs}^2)^{1/2}} - \frac{(a_{cs}k_s+b_{cs})a_{ss}+(c_{cs}k_s+d_{cs})c_{cs}}{(a_{cs}k_s+b_{cs})^2+(c_{cs}k_s+d_{cs})^2}, \quad (108)$$

$$b_{cs} = k_{cp} - m_c(\Delta\omega)^2 + F'(z_0), \tag{109}$$

$$c_{cs} = F'(z_0)[k_{cp} - m_c(\Delta\omega)^2] - \gamma_c\gamma_s(\Delta\omega)^2, \tag{110}$$

$$d_{cs} = \gamma_c(\Delta\omega), \tag{111}$$

$$h_{cs} = \gamma_s k_{cp}(\Delta\omega) - m_c\gamma_s(\Delta\omega)^3 + F'(z_0)(\gamma_c + \gamma_s). \tag{112}$$

It is apparent from Eqs. (97)–(112) that, although the RDF-AFUM signal amplitude *per se* is highly dependent on $F''(z_0)$ and on the cantilever and ultrasonic drive amplitudes F_c and F_s, respectively, the magnitude of the fractional variation $\Delta G_p/G_p$ in the RDF-AFUM signal amplitude resulting from variations in the sample spring constant k_s is independent of F_c, F_s, and $F''(z_0)$. However, $\Delta G_p/G_p$ is dependent upon the values of the cantilever stiffness constant k_{cn} where $n=p$, q, and r, as discussed in Sec. III A. The values of k_{cn} in turn are highly dependent on the choice of cantilever and the frequency chosen to drive the cantilever into resonance. Although $\Delta G_p/G_p$ makes a considerable contribution to image contrast, it is not the only contribution. As with all A-AFM techniques, the resolution of the image digitizer, the dynamic range, and signal-to-noise features of the electronic components, the sharpness of the cantilever tip and the bonding of the ultrasonic transducer among other factors also contribute to the image contrast. The contrast for RDF-AFUM, however, cannot generally exceed that rendered by $\Delta G_p/G_p$. The magnitude of the signal variation for HFM is given by the same equation as for RDF-AFUM except that a single mode may not necessarily dominate the signal. A sum of the largest modal contributions may be appropriate to calculate for HFM the cantilever displacement.

2. Ultrasonic force microscopy

The amplitude of the UFM signal is given by Eqs. (66)–(68). Assuming that Q_{cs} is small compared to Q_{ss} and ε_0, hence negligible in the calculations, we obtain the fractional variation in the cantilever displacement amplitude for the nth mode to be

$$\frac{\Delta\eta_{cn,stat}}{\eta_{cn,stat}} = \left\{ \frac{F'(z_0)k_{cn}}{k_s[k_{cn}k_s + F'(z_0)(k_{cn}+k_s)]} + \frac{F''(z_0)\left(\varepsilon_0\frac{\partial\varepsilon_0}{\partial k_s} + \frac{1}{2}Q_{ss}\frac{\partial Q_{ss}}{\partial k_s}\right)}{F(z_0) + \frac{F''(z_0)}{4}(2\varepsilon_0^2 + Q_{ss}^2)} \right\}_0 \Delta k_s, \tag{113}$$

where Q_{ss} is given by Eq. (61) with $q=n$, $(\partial Q_{ss}/\partial k_s)_0$ by Eq. (98) with $q=n$, ε_0 by Eq. (29), and $(\partial\varepsilon_0/\partial k_s)_0$ by

$$\left(\frac{\partial\varepsilon_0}{\partial k_s}\right)_0 = -\frac{F(z_0)k_{cn}^2}{k_{cn}k_s + F'(z_0)(k_{cn}+k_s)}. \tag{114}$$

3. Atomic force microscopy and force modulation microscopy

For AFAM and FMM, the cantilever displacement amplitude is from Eq. (69) dependent on Q_{cs}, where Q_{cs} is given by Eq. (62). For hard contact, Q_{cs} is given by Eq. (70) and the fractional change in the signal amplitude for mode n is obtained to be

$$\frac{\Delta Q_{cs}}{Q_{cs}} = -\frac{k_{cn} + k_s - m_c\omega_s^2}{(k_{cn} + k_s - m_c\omega_s^2) + (\gamma_c + \gamma_s)^2\omega_s^2}\Delta k_s. \tag{115}$$

The availability and dominance of modes are discussed in Sec. III C.

4. Amplitude modulation–atomic force microscopy

For the AM-AFM hard contact modality, the amplitude is dependent on Q_{cc}, which for hard contact is given by Eq. (78). The fractional change in the amplitude for a given mode n is obtained as

$$\frac{\Delta Q_{cc}}{Q_{cc}} = -\frac{k_{cn} + k_s - m_c\omega_c^2}{(k_{cn} + k_s - m_c\omega_c^2) + (\gamma_c + \gamma_s)^2\omega_c^2}\Delta k_s. \tag{116}$$

It is interesting to note that the variation in amplitude for AM-AFM hard contact is identical to that of AFAM and FMM hard contact except that in AM-AFM the drive frequency is ω_c whereas in AFAM and FMM the drive frequency is ω_s.

C. Summary of acoustic atomic force microscopy modalities and relevant equations

The large number of A-AFM modalities and equations presented in the present work begs that some attempt be made to expedite navigation to relevant equations obtained in the text for a particular A-AFM modality. Such an attempt that gives a summary of equations for signal generation, image phase contrast, and image amplitude contrast relevant to a given A-AFM modality is provided in Table I. Note that for image contrast, different sets of equations are given for the MNR and the hard contrast regime (HCR) of operations. It is advised before using a given equation or set of equations that all sections in the text regarding the chosen A-AFM modality be read to assure that the equations are applied in the proper context.

V. COMPARATIVE MEASUREMENTS USING RESONANT DIFFERENCE-FREQUENCY ATOMIC FORCE ULTRASONIC MICROSCOPY AND AMPLITUDE MODULATION–ATOMIC FORCE MICROSCOPY MAXIMUM NONLINEARITY MODALITIES

In order to test the validity of the present model, comparative measurements of the maximum fractional variation of the Young modulus $\Delta E/E$ in a film of LaRC™-CP2 polyimide polymer were obtained using the RDF-AFUM and AM-AFM maximum nonlinearity modalities. The two modalities represent opposite extremes in measurement complexity, both in instrumentation and in the analytical expressions used to calculate $\Delta E/E$. The polyimide film was 12.7 μm thick and contained a monolayer of gold nanoparticles

TABLE I. Summary of equations given in the text for signal generation, image phase contrast, and image amplitude contrast relevant to a given A-AFM modality. Note that MNR is maximum nonlinearity regime and HCR is hard contact regime.

A-AFM modality	Signal generation equations	Image phase contrast equations	Image amplitude contrast equations
RDF-AFUM HFM	12–15, 54–65	(MNR) 14, 15, 54, 80–90	(MNR) 97–112
UFM	29, 33, 61, 62, 68		(MNR) 29, 61, 98, 113, 114
AFAM FMM	12–15, 58, 62, 69–71	(MNR) 14, 15, 69, 84–86 (HCR) 14, 15, 69, 94	(HCR) 115
AM-AFM	29, 32, 35, 37, 39, 42, 57, 60, 63, 73–79	(MNR) 35, 73, 81, 90–92 (HCR) 77, 93	(HCR) 116

10–15 nm in diameter embedded 7 μm beneath the sample surface. A common scan area of the sample surface was used in obtaining the images. Phase-generated images were obtained in each case. The values of the relevant material and cantilever parameters are[9] $k_s=96.1$ N m^{-1}, $k_{c1}=14$ N m^{-1}, $\gamma_s=4.8\times10^{-5}$ kg s^{-1}, $m_c=3.9\times10^{-12}$ kg, $E=2.4$ GPa, $F'(z_0)=-53$ N m^{-1}, $\omega_c/2\pi=2.1$ MHz, $\omega_s/2\pi=1.8$ MHz, and $\Delta\omega/2\pi=0.3$ MHz.

The variation in the RDF-AFUM phase signal is given from Eq. (54) as $(\Delta\phi_{ss}-\Delta\phi_{cc}+\Delta\beta_{cs}-\Delta\phi_{cs}+\Delta\Gamma+\Delta\chi)$. The maximum phase variation measured in the RDF-AFUM area scan was 13.2°. From Eqs. (14), (15), and (80)–(90), we calculate a value of approximately 24% for the maximum variation in the Young modulus for the material. We point out that the phase contribution $\Delta\chi$ from the gold nanoparticles is of the order 0.1°.

The variation in the phase signal for the AM-AFM maximum nonlinearity mode is given from Eq. (73) as $(-\Delta\phi_{cc}+\Delta\Lambda)$. The maximum phase variation measured over the scan area from the AM-AFM maximum nonlinearity mode was 1.5°. Using the above-stated values of the material and cantilever parameters in Eqs. (90)–(92), we calculate the maximum variation in the Young modulus to be roughly 18%. This value is in good agreement with the value calculated from the RDF-AFUM image. The values of $\Delta E/E$ obtained for the RDF-AFUM and the AM-AFM maximum nonlinearity mode are also in good agreement with a value of roughly 21% obtained from independent mechanical stretching experiments of pure polymer sheets in which the increase in the modulus is attributed to the growth during stretching of a crystalline phase having a larger Young modulus than that of the original amorphous phase.[42]

VI. CONCLUSION

The various modalities of acoustic atomic force microscopy (A-AFM) have become important nanoscale characterization tools for the development of materials and devices. One of the most significant factors affecting all A-AFM modalities is the cantilever tip-sample surface interaction force. We have developed a detailed mathematical model of this interaction that includes a quantitative consideration of the nonlinearity of the interaction force as a function of the cantilever tip-sample surface separation distance. The model makes full use of cantilever beam dynamics and the multiple differentiability of the continuous force-separation curve that results in a set of coupled differential equations, Eqs. (17) and (18), for the displacement amplitudes of both the cantilever and the sample surface. The coupled dynamical equations are recast in matrix form and solved by a standard iteration procedure. Only flexural vibrations of the cantilever and out-of-plane oscillations of the sample surface are considered in the present derivation.

We again point out that Eqs. (17) and (18) are obtained assuming that the cantilever is a rectangular beam of constant cross section, the dynamics of which are characterized by a set of eigenfunctions that form an orthogonal basis for the solution set. For some other cantilever shape, a different orthogonal basis set of eigenfunctions would be appropriate. However, the mathematical procedure used here would lead again to Eqs. (17) and (18) with values of the coefficients appropriate to the different cantilever geometry. Practicably, this means that the shape of the cantilever is not as important in the solution set as knowing the cantilever modal resonant frequencies, obtained experimentally. The modal frequencies and solution set are expanded to include nonlinear modes generated by nonlinear interaction forces or large cantilever drive amplitudes.

A general steady-state solution of the coupled dynamical equations that accounts for the positions of the excitation force (e.g., a piezotransducer) and the cantilever tip along the length of the cantilever and for the position of the laser probe on the cantilever surface is found. The solution is applied to various A-AFM modalities including the commonly used amplitude modulation–atomic force microscopy mode, force

modulation microscopy, atomic force acoustic microscopy, ultrasonic force microscopy, heterodyne force microscopy, and resonant difference-frequency atomic force ultrasonic microscopy. Image generation and contrast equations are obtained for each of the aforementioned A-AFM modalities assuming for expediency that the contrast results only from variations in the sample stiffness constant. Since the sample stiffness constant is related directly to the Young modulus of the sample, the contrast can be expressed in terms of the variation in the Young modulus from point to point as the sample is scanned. We note further the existence of two values of the sample stiffness constant, corresponding to the attractive and repulsive regimes of the force-separation curve. The two values allow for a bistability in the cantilever oscillations that is experimentally observed.[26]

Equations for both the maximum nonlinearity regime and the hard contact (linear) regime of cantilever engagement with the sample surface are obtained. For A-AFM operation outside these regimes, it is necessary to use all terms in the solution set given in Sec. II to describe the signal output. It is worthwhile to reiterate the caution given in Sec. IV A 2. The extent to which the hard contact (linear regime) equations apply depends on how well the approximation $F'(z_0) \rightarrow -\infty$ holds. In those cases where such an assumption is suspect, all terms in the equations for a given modality should be used.

In order to test the validity of the present model, comparative measurements of the maximum fractional variation of the Young modulus $\Delta E/E$ in a film of LaRC™-CP2 polyimide polymer were obtained from phase-generated images using the RDF-AFUM and AM-AFM maximum nonlinearity modalities. The two modalities represent opposite extremes in measurement complexity, both in instrumentation and in the analytical expressions used to calculate $\Delta E/E$. The values of 24% calculated for RDF-AFUM and 18% calculated for the AM-AFM maximum nonlinearity mode are in remarkably close agreement for such disparate techniques. The agreement of both calculations with the value of 21% obtained from independent mechanical stretching experiments of LaRC™-CP2 sheet material offers strong evidence for the validity of the present model.

The present model can also be used to quantify the image contrast from variations in the sample damping coefficient γ_s or from a combination of damping coefficient and Young modulus variations in the material. Space limitations prohibit the inclusion of such contrast mechanisms here, but the effects can be derived straightforwardly by the reader from the equations derived in Sec. II. Although the present model is developed for flexural oscillations of the cantilever and out-of-plane vibrations of the sample surface, the model can in principle be extended to include other modes of cantilever oscillation and sample surface response. It is anticipated that such a development would provide even greater opportunities for obtaining quantitative information on material properties using the various A-AFM modalities.

*john.h.cantrell@nasa.gov
†sac3k@virginia.edu

[1] G. Binnig, C. F. Quate, and Ch. Gerber, Phys. Rev. Lett. **56**, 930 (1986).
[2] P. Maivald, H. J. Butt, S. A. Gould, C. B. Prater, B. Drake, J. A. Gurley, V. B. Elings, and P. K. Hansma, Nanotechnology **2**, 103 (1991).
[3] U. Rabe and W. Arnold, Appl. Phys. Lett. **64**, 1493 (1994).
[4] U. Rabe, S. Amelio, M. Kopychinska, S. Hirsekorn, M. Kempf, M. Goken, and W. Arnold, Surf. Interface Anal. **33**, 65 (2002).
[5] O. Kolosov and K. Yamanaka, Jpn. J. Appl. Phys., Part 2 **32**, L1095 (1993).
[6] K. Yamanaka, H. Ogiso, and O. Kolosov, Appl. Phys. Lett. **64**, 178 (1994).
[7] M. T. Cuberes, H. E. Alexander, G. A. D. Briggs, and O. V. Kolosov, J. Phys. D **33**, 2347 (2000).
[8] G. S. Shekhawat and V. P. Dravid, Science **310**, 89 (2005).
[9] S. A. Cantrell, J. H. Cantrell, and P. T. Lillehei, J. Appl. Phys. **101**, 114324 (2007).
[10] L. Muthuswami and R. E. Geer, Appl. Phys. Lett. **84**, 5082 (2004).
[11] D. C. Hurley, K. Shen, N. M. Jennett, and J. A. Turner, J. Appl. Phys. **94**, 2347 (2003).
[12] R. E. Geer, O. V. Kolosov, G. A. Briggs, and G. S. Shekhawat, J. Appl. Phys. **91**, 4549 (2002).
[13] Oleg V. Kolosov, M. R. Castell, C. D. Marsh, G. A. Briggs, T. I. Kamins, and R. S. Williams, Phys. Rev. Lett. **81**, 1046 (1998).
[14] G. G. Yaralioglu, F. L. Degertekin, K. B. Crozier, and C. F. Quate, J. Appl. Phys. **87**, 7491 (2000).
[15] Y. Zheng, R. E. Geer, K. Dovidenko, M. Kopycinska-Müller, and D. C. Hurley, J. Appl. Phys. **100**, 124308 (2006).
[16] M. Kopycinska-Müller, R. H. Geiss, and D. C. Hurley, Ultramicroscopy **106**, 466 (2006).
[17] L. Nony, R. Boisgard, and J. P. Aime, J. Chem. Phys. **111**, 1615 (1999).
[18] K. Yagasaki, Phys. Rev. B **70**, 245419 (2004).
[19] H.-L. Lee, Y.-C. Yang, W.-J. Chang, and S.-S. Chu, Jpn. J. Appl. Phys., Part 1 **45**, 6017 (2006).
[20] J. Kokavecz, O. Marti, P. Heszler, and A. Mechler, Phys. Rev. B **73**, 155403 (2006).
[21] K. Wolf and O. Gottlieb, J. Appl. Phys. **91**, 4701 (2002).
[22] J. A. Turner, J. Sound Vib. **275**, 177 (2004).
[23] R. W. Stark and W. M. Heckl, Rev. Sci. Instrum. **74**, 5111 (2003).
[24] R. W. Stark, G. Schitter, M. Stark, R. Guckenberger, and A. Stemmer, Phys. Rev. B **69**, 085412 (2004).
[25] H. Hölscher, U. D. Schwarz, and R. Wiesendanger, Appl. Surf. Sci. **140**, 344 (1999).
[26] R. Garcia and R. Perez, Surf. Sci. Rep. **47**, 197 (2002).
[27] L. Meirovitch, *Analytical Methods in Vibrations* (Macmillan, New York, 1967).
[28] I. S. Sokolnikoff and R. M. Redheffer, *Mathematics of Physics and Modern Engineering* (McGraw-Hill, New York, 1958).
[29] R. G. Parr and W. Yang, *Density-Functional Theory of Atoms*

and Molecules (Oxford University Press, New York, 1989).
[30] R. B. Leighton, *Principles of Modern Physics* (McGraw-Hill, New York, 1959).
[31] G. Burns, *Solid State Physics* (Academic, San Diego, CA, 1989).
[32] B. M. Law and F. Rieutord, Phys. Rev. B **66**, 035402 (2002).
[33] M. A. Lantz, H. J. Hug, R. Hoffmann, P. J. A. van Schendel, P. Kappenberger, S. Martin, A. Baratoff, and H.-J. Güntherodt, Science **291**, 2580 (2001).
[34] J. Polesel-Maris, A. Piednoir, T. Zambelli, X. Bouju, and S. Gauthier, Nanotechnology **14**, 1036 (2003).
[35] T. Eguchi and Y. Hasegawa, Phys. Rev. Lett. **89**, 266105 (2002).
[36] M. Saint Jean, S. Hudlet, C. Guthmann, and J. Berger, J. Appl. Phys. **86**, 5245 (1994).
[37] H. B. Chan, V. A. Aksyuk, R. N. Kleiman, D. J. Bishop, and F. Capasso, Phys. Rev. Lett. **87**, 211801 (2001).
[38] J. H. Cantrell, J. Appl. Phys. **96**, 3775 (2004).
[39] D. C. Wallace, in *Solid State Physics*, edited by H. Ehrenreich, F. Seitz, and D. Turnbull (Academic, New York, 1970), Vol. 25, p. 301.
[40] R. B. Thompson and H. F. Tiersten, J. Acoust. Soc. Am. **62**, 33 (1977).
[41] L. I. Schiff, *Quantum Mechanics* (McGraw-Hill, New York, 1968).
[42] C. C. Fay, D. M. Stoakley, and A. K. St. Clair, High Perform. Polym. **11**, 145 (1999).